JACS
JOURNAL OF THE AMERICAN CHEMICAL SOCIETY
Article
Cite This: J. Am. Chem. Soc. 2018, 140, 244−249
pubs.acs.org/JACS

NFGAIL Amyloid Oligomers: The Onset of Beta-Sheet Formation and the Mechanism for Fibril Formation

Waldemar Hoffmann,[†,‡] Kristin Folmert,[†] Johann Moschner,[†] Xing Huang,[‡] Hans von Berlepsch,[†] Beate Koksch,[†] Michael T. Bowers,[§] Gert von Helden,[‡] and Kevin Pagel*[,†]

[†]Freie Universität Berlin, Institute of Chemistry and Biochemistry - Organic Chemistry, Takustr. 3, 14195 Berlin, Germany
[‡]Fritz-Haber-Institut der Max-Planck-Gesellschaft, Faradayweg 4-6, 14195 Berlin, Germany
[§]Department of Chemistry and Biochemistry, University of California Santa Barbara, Santa Barbara, California 93106, United States

Supporting Information

ABSTRACT: The hexapeptide NFGAIL is a highly amyloidogenic peptide, derived from the human islet amyloid polypeptide (hIAPP). Recent investigations indicate that presumably soluble hIAPP oligomers are one of the cytotoxic species in type II diabetes. Here we use thioflavin T staining, transmission electron microscopy, as well as ion mobility-mass spectrometry coupled to infrared (IR) spectroscopy to study the amyloid formation mechanism and the quaternary and secondary structure of soluble NFGAIL oligomers. Our data reveal that at neutral pH NFGAIL follows a nucleation dependent mechanism to form amyloid fibrils. During the lag phase, highly polydisperse, polymorph, and compact oligomers (oligomer number n = 2−13) as well as extended intermediates (n = 4−11) are present. IR secondary structural analysis reveals that compact conformations adopt turn-like structures, whereas extended oligomers exhibit a significant amount of β-sheet content. This agrees well with previous molecular dynamic simulations and provides direct experimental evidence that unordered off-pathway NFGAIL aggregates up to the size of at least the 13-mer as well as partially folded β-sheet containing oligomers are coexisting.

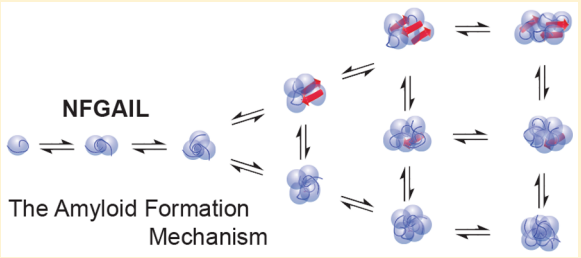

1. INTRODUCTION

Amyloid formation is a hallmark of various diseases such as type II diabetes (T2D), Parkinson's, and Alzheimer's disease. In the case of T2D, unstructured human islet amyloid polypeptide (hIAPP) monomers assemble into highly structured, β-sheet-rich, insoluble deposits known as amyloid plaques.[1] These plaques are found in more than 95% of T2D patients, which suggests their direct involvement in β-cell dysfunction in the pancreas.[2−5] Recent studies have shown that especially early hIAPP oligomers represent the toxic species.[1,5−7] Understanding their detailed structure and the mechanism leading from monomer to fibrils is crucial to selectively modulate the assembly pathway.[1,7−10]

Aggregation prone domains of hIAPP include the fragments 1−8, 8−20, 20−29, and 30−37, all of which form amyloid fibrils.[11−15] While each of these fragments may play a role in the assembly of the parent hIAPP, the 20−29 region has garnered the most attention, since chemical modification[16,17] or mutations[5] in this region disrupt fibril formation. The 22NFGAIL27 fragment within this region is the shortest known hIAPP sequence capable of forming amyloid fibrils at pH ∼ 7 and was shown to be cytotoxic towards the pancreatic cell line RIN5fm.[18] In addition, recent evidence suggests the 20−29 domain may play a central role in fibril formation of full-length hIAPP.[19] Thus, many experimental[20−22] as well as theoretical[23−28] studies have investigated the assembly characteristics of NFGAIL. They show that the ionic strength[23] influences the NFGAIL assembly and oligomers are formed due to attractive, hydrophobic interactions between phenylalanine residues.[22,25,26,28] Molecular dynamic simulations further support that hydrophobic interactions lead to the formation of both disordered and structured aggregates.[24,26] However, the dissociation of those disordered oligomers is the rate-limiting step for the formation of structured aggregates.[27] Those can then further evolve into amyloid fibrils composed of antiparallel β-strands.[22,28] The characterization of soluble oligomers using solution-based Fourier transform-infrared (FT-IR), circular dichroism (CD), or nuclear magnetic resonance (NMR) spectroscopy only provides ensemble averaged information rather than information on individual oligomeric states. Thus, experimental evidence for the proposed assembly is still missing.

Gas-phase techniques can isolate and characterize a single species in the presence of many others without affecting the underlying equilibrium. In particular, ion mobility-mass spectrometry (IM-MS), a technique which separates ions based on their mass, charge, size, and shape, has long been applied successfully to study the structure and aggregation of reacting systems[29] and more recently has been used to follow

Received: September 12, 2017
Published: December 13, 2017

DOI: 10.1021/jacs.7b09510
J. Am. Chem. Soc. 2018, 140, 244−249

the assembly of early amyloid intermediates.[30−33] In a typical IM-MS experiment, the analyte is first carefully transferred from solution into the gas phase using soft ionization techniques such as electrospray ionization (ESI). These techniques have been shown to preserve solution backbone structures of peptides and small proteins[34−37] and aggregates of hexameric peptides[38] and Aβ peptides.[39] Transferred ions are then gently pulsed into an IM cell that is filled with an inert buffer gas, through which they move under the influence of a weak electric field. Compact ions undergo fewer collisions with the buffer gas than extended ions and therefore leave the IM cell earlier. The resulting drift time can further be used to calculate a rotationally averaged collision cross section (CCS), which is an instrumentally independent value from which information about the quaternary structure of amyloid oligomers can be deduced.[38]

IR spectroscopy on the other hand is highly dependent on intramolecular vibrations, which makes it an ideal tool to obtain detailed structural information.[40] For example, the amide I band, i.e., the C═O stretching mode, strongly depends on the secondary structure adopted by peptides and proteins.[41,42] Antiparallel β-sheet-rich proteins typically feature an amide I frequency at lower wavenumbers (1610−1640 cm^{-1}) and an additional weak mode at higher wavenumbers (~1700 cm^{-1}) compared to helical or turn-like structures (1648−1670 and ~1660−1690 cm^{-1}, respectively).[37,41,42] Recently, IM-MS was successfully used as a preselection tool to perform gas-phase IR spectroscopy on individual amyloid oligomeric states and conformations.[43] The data showed that the tetramers (n = 4) of the two amyloid forming peptides VEALYL and YVEALL undergo a characteristic transition from compact and unordered conformations into more extended and β-sheet-rich versions.[43] All of the observed higher-order oligomers ($n \geq 4$) were shown to exhibit an elevated β-sheet content. Here, we employ IM-MS coupled to gas-phase IR spectroscopy for the structural characterization of NFGAIL oligomers.

2. RESULTS AND DISCUSSION

The hexapeptide NFGAIL is the shortest fragment of hIAPP known to form amyloid fibrils at neutral pH.[18] Those fibrils have been shown to feature antiparallel β-strands and a morphology similar to full length hIAPP fibrils.[21,28,44] In order to study the tendency of early oligomers to form β-sheets, the NFGAIL peptide was incubated for two days in ammonium acetate buffer. This procedure lead to the formation of fibrillar aggregates with anisometric cross section, a mean apparent diameter of 20−30 nm, and a few hundreds of nanometers length (Figure 1a and b). Typical protofilaments have not been detected. The kinetics of fibril formation was monitored in real-time using thioflavin T (ThT) assay.[45] ThT intercalates into the cavity of amyloid fibrils, which leads to an increased fluorescence. Even for high concentrations (4 mM), the hexapeptide NFGAIL follows a nucleation dependent growth mechanism (Figure S2), characteristic of classical on-pathway amyloid formation. The sigmoidal growth behavior can be divided into lag, growth, and saturation phases. During the lag phase (20 h), early soluble NFGAIL intermediates are present.[7,18] These transient oligomers are highly polydisperse, i.e., a multitude of oligomeric states coexist. In addition, they most likely are polymorph; i.e., they occupy a wide range of different conformations for one oligomeric state. All species can interconvert or undergo subunit exchange, but once a so-called nucleus is formed, the autocatalytical growth phase is initiated. The nuclei presumably act as a template to assemble monomers into mature fibrils, which are present at the saturation phase (see ref 39 for an example).

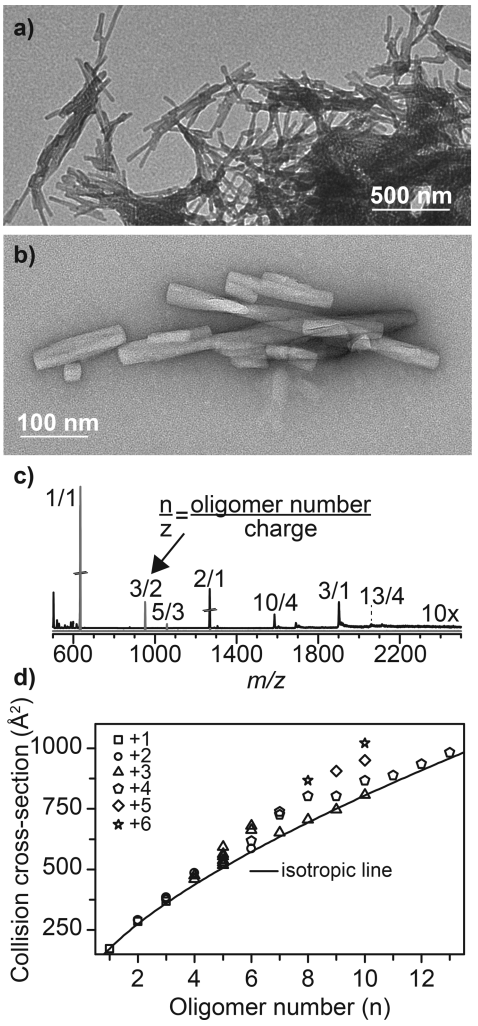

Figure 1. Structural investigation of NFGAIL oligomers. (a, b) Negative staining transmission electron microscopy (TEM) images of a NFGAIL solution (4 mM) in ammonium acetate buffer (10 mM, pH ~ 7) show the formation of amyloid fibrils. Scale bars: (a) 500 nm, (b) 100 nm. (c) Mass spectra recorded at two different instrumental settings on the iMob[46] instrument (gray and black line) indicate for a freshly electrosprayed NFGAIL solution the presence of multiple oligomers, with n being the oligomer number and z the charge. (d) Measured collision cross sections (CCSs) as a function of the oligomer number n. The solid line indicates theoretical CCSs expected for an idealized spherical growth. The experimental error of each CCS measurement is less than 1% and smaller than the size of the symbols.

The mass spectrum (Figure 1c) shows that NFGAIL immediately forms a wide distribution of oligomers, spanning from a singly charged monomer n/z = 1/1 (with n = oligomer number, z = charge) up to a quadruply charged 13-mer n/z = 13/4. All of these oligomers carry much less charge than their number of peptide strands and are therefore most likely not disturbed by Coulomb repulsion and derived from solution. IM-MS further reveals that multiple conformations and higher oligomeric states of the same m/z value exist (Figures S3, S4, and S5). CCSs of all these species (Table S4) are displayed as

DOI: 10.1021/jacs.7b09510
J. Am. Chem. Soc. 2018, 140, 244−249

a function of the oligomer number in Figure 1d. The solid line represents an ideal isotropic (i.e., globular) growth behavior, following the equation $\sigma = \sigma_1 \cdot n^{2/3}$, where σ_1 is the monomer's CCS and n the oligomer number.[38] Oligomers exhibiting an experimental CCS on the isotropic line adopt compact, spherical conformations consisting of turn-like and/or unordered structures. Extended oligomers that are deviating from the isotropic growth model on the other hand are often partially structured and form helical or β-sheet-rich conformations.[38,43] Figure 1d shows a variety of compact (experimental CCSs close to the isotropic line) NFGAIL oligomers, starting from the singly charged monomer (n/z = 1/1) up to the quadruply charged 13-mer (n/z = 13/4). These compact oligomers presumably adopt turn-like or unordered conformations. Interestingly, starting from the tetramer (n = 4), multiple conformations are present. For example, for the pentamer, these range from compact (n/z = 5/2 with 523 Å^2 and n/z = 5/3 with 520 Å^2) to highly extended structures (n/z = 5/3 with 540 and 566 Å^2, respectively). Similar extended conformations are also observed for higher oligomeric states (n = 6−10). Thus, the NFGAIL tetramer might represent a structural transition point from unordered/turn-like conformations into at least partially folded, presumably β-sheet-rich structures. This observation is consistent with recent results on the 8−20 fragment where a significant β-sheet content begins at the tetramer.[47] In full-length hIAPP, however, a β-hairpin conformer is observed for both the monomer and dimer[30,48] and is shown to be the conformation that leads to fibrilization. Further, a multidimensional analytical approach for the full-length hIAPP shows that in the presence of copper ions globular and toxic off-pathway hIAPP oligomers are formed, but in neat hIAPP, a different assembly pathway starting at tetramer is observed.[49] Another IM-MS study also observed more extended hIAPP versions for $n \geq 4$.[50]

Although IM-MS provides information on the stoichiometry and overall size of amyloid oligomers, direct details of the fine structure cannot be deduced. Instead, IM-MS can be used to preselect individual conformations for a subsequent analysis by orthogonal techniques such as gas-phase IR spectroscopy. The combination of IM-MS and IR spectroscopy allows the individual characterization of m/z- and drift-time-selected species on the quaternary- as well as the secondary-structure level. Amide I vibrations (C═O stretching modes) are highly sensitive towards the secondary structure adopted by peptides and proteins.[37,41,42] However, due to the number of vibrational modes, individual amide I features usually overlap. In conventional condensed-phase spectroscopy, a deconvolution procedure is typically used to deduce the relative content of each motif.[51,52] In contrast, such relative populations cannot be directly obtained from gas-phase infrared multiple photon dissociation (IRMPD) spectra without making assumptions about the oscillator strengths. The IRMPD process is based on the sequential absorption of multiple photons, and the resulting IR intensity does not scale linearly with the number of absorbed photons. A deconvolution of IRMPD spectral features may therefore not be fully quantitative but still represents a reasonably good representation of the different structural features contributing to a complex spectral band. Hence, while we provide "quantitative" percentages of β-sheet content in a given band, these actually represent the relative amounts between spectral bands for differing conformations or oligomeric systems but are less quantitative within a given band.

Figure 2 shows a set of IRMPD spectra of compact NFGAIL oligomers (n = 2−11) measured in the wavenumber range

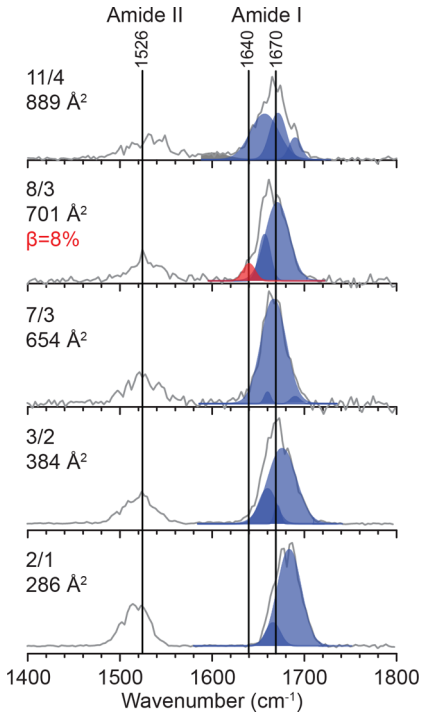

Figure 2. Infrared multiple photon dissociation (IRMPD) spectra of m/z- and drift-time-selected compact NFGAIL oligomers, exhibiting experimental CCSs similar to theoretical values predicted by the isotropic growth model. Fractions of the amide I band that are representative for β-sheet structures (1600−1640 cm^{-1}) and turn-like structures (1660−1685 cm^{-1}) are shown in red and blue, respectively. For details about the fitting procedure, see the Supporting Information.

from 1400 to 1800 cm^{-1}. All spectra feature two bands assigned as amide II (1480−1540 cm^{-1}) and amide I (1600−1720 cm^{-1}). The amide I region was fitted with multiple Gaussian curves (for details, see the Supporting Information), where antiparallel β-sheets and turn-like motifs are labeled in red and blue, respectively. The center of the amide I band of the singly charged dimer (n/z = 2/1) appears at 1683 cm^{-1}, whereas for higher oligomers (n = 3−11) this feature occurs at lower wavenumbers. The extent of hydrogen bonding within the dimer is apparently lower than that for larger oligomers and therefore provides less perturbation for the individual C═O oscillators. The amide I band of higher compact oligomers appears around 1670 cm^{-1}, which is indicative for turn-like structures.[41−43] This observation agrees with the fact that the experimental CCSs of these oligomers represent compact, spherical structures. Interestingly, an additional shoulder around 1640 cm^{-1} emerges for the triply charged octamer (n/z = 8/3), indicating a β-sheet content of approximately 8%. The experimental CCS of this octamer (n/z = 8/3 with 701 Å^2), however, fits well with the theoretical value for a spherical, compact conformation (694 Å^2). A small β-sheet content observed via IRMPD may not necessarily be correlated with an extended structural ensemble.

The first NFGAIL oligomers that considerably deviate from the isotropic line are pentamers. They are highly polymorph and range from compact (n/z = 5/2 with 523 Å^2 and n/z = 5/3 with 520 Å^2) to highly extended (n/z = 5/3 with 540 and

DOI: 10.1021/jacs.7b09510
J. Am. Chem. Soc. 2018, 140, 244−249

566 Å^2) conformations. The individual, conformer-selective IR spectra show an amide I band at 1674 cm^{-1}, which indicates a predominantly turn-like structure present for all pentamers (Figure 3). Interestingly, the more extended pentamer

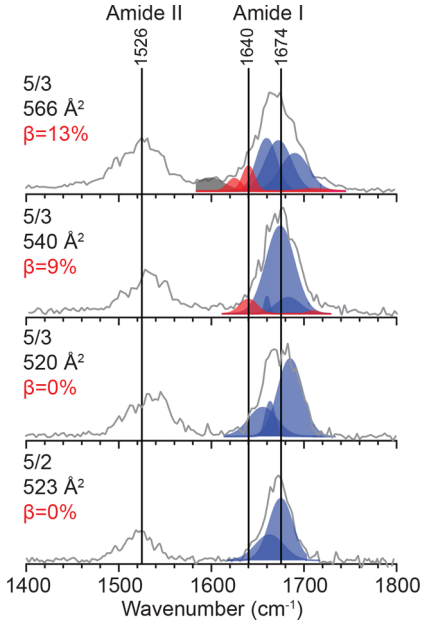

Figure 3. Infrared multiple photon dissociation (IRMPD) spectra of m/z- and drift-time-selected NFGAIL pentamers ranging from compact (n/z = 5/2 with 523 Å^2 and n/z = 5/3 with 520 Å^2) to extended (n/z = 5/3 with 540 Å^2 and 566 Å^2, respectively) structures. The amide I band (1600−1700 cm^{-1}) was deconvoluted with multiple Gaussians representing β-sheets (red) or turn-like (blue) conformations. One additional Gaussian between 1560 and 1600 cm^{-1} (gray) was included to compensate for an overlapping amide I and amide II band. Details of the fitting procedure are given in the Supporting Information.

isoforms exhibit a broader amide I band than that observed for the corresponding compact species and show additional features at around 1620−1640 and 1700 cm^{-1} (red Gaussians). These features are indicative of antiparallel β-strands. An amide I deconvolution reveals a β-sheet IR fraction of up to 13%. This observation is in good agreement with previous results, which suggest a higher β-sheet content for more extended conformations.[38,43] As a result of the non-linear IR absorption process, however, it is not possible to absolutely quantify how many single peptide strands within the NFGAIL pentamer contribute to the β-sheet fraction in the IR spectrum. For a short peptide such as NFGAIL, the β-sheet IR fraction originates from the noncovalent assembly of at least two individual peptide strands. In addition, a recent 2D-IR study on the full-length hIAPP further suggests that β-sheet-rich hIAPP oligomers, which are present in the lag phase, are composed of less than four β-strands.[19] Thus, the here investigated NFGAIL oligomers are likely to be composed of at least two or three β-strands.

The gas-phase IR spectra of other extended NFGAIL oligomers (n = 4−9) also show a broad amide I band, with elevated intensities at 1617−1640 cm^{-1} (Figure 4). The Gaussian deconvolution analysis reveals a significant β-sheet content of up to 24%. There is a significant jump in β-sheet content from n = 4 (14%) to n = 7 (24%) but no smooth trend as n increases. Hence, factors beyond oligomer size contribute

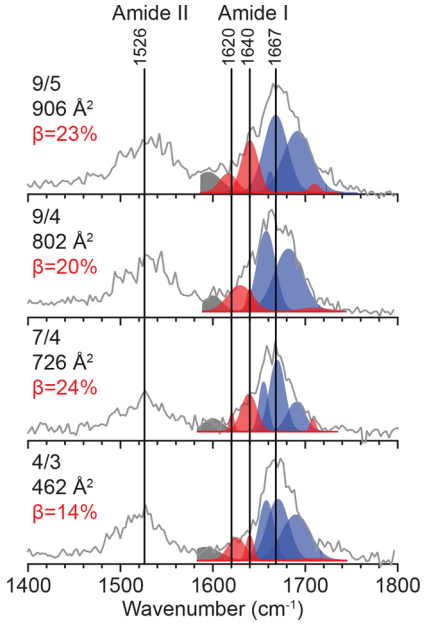

Figure 4. Individual infrared multiple photon dissociation (IRMPD) spectra of extended NFGAIL oligomers. The amide I band (1600−1700 cm^{-1}) was deconvoluted with multiple Gaussians representing β-sheets (red) or turn-like (blue) conformations. Details of the fitting procedure are given in the Supporting Information.

to β-sheet formation. A complex equilibrium between oligomeric states and conformations with different β-sheet content is established in the early stages of NFGAIL aggregation (lag phase). Secondary structural transitions might therefore occur over a multitude of oligomeric states, as observed for other amyloid forming sequences such as NNQQNY.[38] Similarly to NFGAIL, also the full-length hIAPP peptide shows a diverse free energy landscape, which is more complicated than a simple transition from a random-coil structure into a perfect fiber-like nucleus.[19] Thus, the short NFGAIL peptide might serve as a good model system and provides critical insights into the full-length hIAPP assembly mechanism. In addition, the coexistence of both turn-like as well as partially β-sheet-rich structured aggregates for n = 4−10 is in agreement with a previous theoretical study, which showed that unstructured NFGAIL oligomers are initially formed and their subsequent dissociation is the rate-limiting step for the assembly into higher, β-sheet-rich oligomers.[27] The extended β-sheet-rich NFGAIL oligomers investigated here, therefore, most likely represent on-pathway oligomers to amyloid fibrils.

3. CONCLUSIONS

A combination of condensed-phased methods such as ThT assay and TEM as well as gas-phase methods such as IM-MS coupled to gas-phase IR spectroscopy was used to study the kinetics and oligomeric structural evolution occurring in NFGAIL fibril formation. Under buffered conditions, NFGAIL follows a nucleation dependent growth mechanism into mature fibrils. IM-MS analysis reveals that during the lag phase a variety of oligomeric states n and different conformations ranging from compact (for n = 2−13) to extended (for n = 4−10) structures are present. Interestingly, also for the full-length hIAPP peptide[49,50] and other amyloid forming systems,[38,43,48,53] a similar transition from compact to more

DOI: 10.1021/jacs.7b09510
J. Am. Chem. Soc. 2018, 140, 244−249

extended versions has been observed. In all cases, the conversion typically starts for oligomers as little as two to nine subunits.[49,50] The early transition into more extended, presumably β-sheet-rich structures might be therefore a general feature of amyloid forming systems.

The gas-phase IR analysis of compact NFGAIL oligomers (n = 2−11) shows an amide I band centered at 1670 cm^{-1}, associated with turn-like structures. Extended NFGAIL oligomers (n = 4−9), however, exhibit additional IR features at 1617−1640 cm^{-1}, which are representative of β-sheet-rich structures. Deconvolution of the amide I band indicates a β-sheet IR content of up to 24% for extended NFGAIL oligomers.

A previous theoretical study suggests that the formation of unstructured aggregates and their subsequent dissociation is the rate-limiting step to form higher-order, β-sheet-rich NFGAIL oligomers.[27] The data presented here support this hypothesis by providing the first direct secondary structure data for individual oligomers. Due to the complex assembly disassembly assembly cascade, the investigated oligomers range from largely unordered to significantly folded β-sheet-containing species, and therefore, for every extended version, a more compact, unordered counterpart coexists. The conformational complexity for each NFGAIL oligomer observed here is in contrast to our previous study[43] on VEALYL and YVEALL where conformational complexity was limited to only one or two oligomer sizes. This points to coexistence of on- and off-pathway aggregates in the NFGAIL system and complex assembly/disassembly dynamics that ultimately leads to both an on-pathway β-sheet dominated set of oligomers leading to fibrils and an off-pathway more isotropic set of oligomers up to at least the size of a 13-mer.

4. MATERIALS AND METHODS

4.1. Samples. The hexapeptide NFGAIL was synthesized manually according to standard Fmoc chemistry using a preloaded TGA resin. Peptide purification was performed on a low-pressure HPLC system. Purity was validated using an analytical HPLC system and high-resolution mass spectrometry (Figure S1). Further details can be found in the Supporting Information.

4.2. ThT Assay. An NFGAIL stock solution was prepared by dissolving the purified NFGAIL in HFIP (1,1,1,3,3,3-hexafluoro-2-propanol) (~18 mM) and was further sonicated for 15 min to dissolve all preformed aggregates. Aliquots of this stock solution were dried and then redissolved to a final concentration of 4 mM in ammonium acetate buffer (10 mM, pH ~ 7), containing 20 μM ThT. After dissolution, the sample was sonicated for 30 s and then incubated at 37 °C with 1300 rpm.

Fluorescence spectra were recorded using a 1 cm path length quartz cuvette (Hellma, Müllheim, Germany) and a luminescence spectrometer LS50B (PerkinElmer, Boston, MA, USA). Spectra were recorded at room temperature from 470 to 500 nm after excitation at 420 nm (excitation slit width 5 nm; emission slit width 10 nm; scan speed = 300 nm/min; accumulations = 3). The fluorescence intensity at 485 nm was normalized with respect to its maximum value.

4.3. TEM Characterization. Sample preparation was performed according to ThT assay. The solution was further incubated at 37 °C and shaken with 1300 rpm for 2 days. During the incubation time, the formation of insoluble deposition was observed. Samples for staining electron microscopy were prepared by adsorbing 5 μL aliquots of peptide solution to glow-discharged carbon-coated collodium films on 400-mesh copper grids. The grids were blotted, stained with 1% phosphotungstic acid, and air-dried. TEM micrographs were taken by a FEI Talos L120 TEM operated at 120 kV for morphological characterization.

4.4. Isomer-Selective IR Spectroscopy. The purified peptide was dissolved in ammonium acetate (10 mM, pH ~ 7) to yield a final peptide concentration of 1 mM. For nESI, ~8 μL of sample was loaded into in-house-prepared Pd/Pt-coated borosilicate capillaries, and voltages of 0.6−1.0 kV were applied.

The ion mobility method for drift-time-based selection is well established.[54] Ions are drift-time-preselected prior to irradiation with intense IR light using an in-house constructed drift-tube ion mobility-mass spectrometer similar to one described previously.[40,55] After ions are generated using a *nano* electrospray ionization (nESI) source, they are transferred and stored in an entrance funnel. Subsequently, ions are released by 150 μs long pulses into a drift tube, where they travel under the influence of a weak electric field (10−20 V/cm) through helium buffer gas (~4 mbar). The drift velocity of a particular ion depends on its mobility, which in turn is based on its overall size, shape, and charge. After releasing the ion mobility cell, ions are mass-selected using a quadrupole mass filter and their arrival time distributions (ATDs) can be recorded by measuring the time dependent ion current of the m/z-selected species after release of the ion trap. CCSs are measured on two different IMS instruments: (1) HiRes[55] located in Santa Barbara (resolution, R = 100), which allows a high IMS separation of individual conformations; (2) iMob[46] located in Berlin (R = 40), which is connected to a free electron laser and therefore allows the recording of conformer- and mass-selected IR spectra.

Gas-phase IR spectra are recorded on the iMob[46] instrument by selecting a narrow drift-time window (100 μs width) using electrostatic deflection prior to mass selection. This m/z- and ion-mobility-selected ion cloud was further irradiated by an intense (10−40 mJ) 10 μs pulse of IR photons. The photofragmentation is detected by a time-of-flight (ToF) mass analyzer, and IR spectra are obtained by plotting the fragmentation yield as a function of the tunable IR wavenumber. The final IR spectrum represents an average of at least two individual scans, where each scan was obtained by scanning in 3 cm^{-1} wavenumber steps and averaging at least 40 spectra for each step.

The tunable mid-IR light is provided by the Fritz-Haber-Institut free electron laser and is transported to the instrument via an evacuated beamline. The last two meters of the beamline are flushed with dry nitrogen to avoid water absorption.

■ ASSOCIATED CONTENT

Supporting Information

The Supporting Information is available free of charge on the ACS Publications website at DOI: 10.1021/jacs.7b09510.

Details of the synthesis protocol, peptide purification, experimental procedures, data from ion mobility-mass spectrometry, collision cross sections, and Gaussian fitting routines (PDF)

■ AUTHOR INFORMATION

Corresponding Author

*kevin.pagel@fu-berlin.de

ORCID

Xing Huang: 0000-0002-8700-0606
Beate Koksch: 0000-0002-9747-0740
Gert von Helden: 0000-0001-7611-8740
Kevin Pagel: 0000-0001-8054-4718

Notes

The authors declare no competing financial interest.

■ ACKNOWLEDGMENTS

M.T.B. gratefully acknowledges support from the US National Science Foundation under Grant No. CHE-1565941 and the Alexander von Humboldt foundation. W.H. gratefully acknowl-

DOI: 10.1021/jacs.7b09510
J. Am. Chem. Soc. 2018, 140, 244−249

edges financial support from the German Academic Exchange Service (DAAD). J.M. gratefully acknowledges financial support from the DFG grant SFB 1114. We thank Mateusz Marianski for proofreading the manuscript.

REFERENCES

(1) Cao, P.; Abedini, A.; Raleigh, D. P. *Curr. Opin. Struct. Biol.* **2013**, *23*, 82.
(2) Clark, A.; Cooper, G. J.; Lewis, C. E.; Morris, J. F.; Willis, A. C.; Reid, K. B.; Turner, R. C. *Lancet* **1987**, *330*, 231.
(3) Luskey, K. L. *Diabetes Care* **1992**, *15*, 297.
(4) Kahn, S. E.; Andrikopoulos, S.; Verchere, C. B. *Diabetes* **1999**, *48*, 241.
(5) Cao, P.; Marek, P.; Noor, H.; Patsalo, V.; Tu, L. H.; Wang, H.; Abedini, A.; Raleigh, D. P. *FEBS Lett.* **2013**, *587*, 1106.
(6) Lin, C.-Y.; Gurlo, T.; Kayed, R.; Butler, A. E.; Haataja, L.; Glabe, C. G.; Butler, P. C. *Diabetes* **2007**, *56*, 1324.
(7) Haataja, L.; Gurlo, T.; Huang, C. J.; Butler, P. C. *Endocr. Rev.* **2008**, *29*, 303.
(8) Cooper, G. J.; Willis, A. C.; Clark, A.; Turner, R. C.; Sim, R. B.; Reid, K. B. *Proc. Natl. Acad. Sci. U. S. A.* **1987**, *84*, 8628.
(9) Lorenzo, A.; Razzaboni, B.; Weir, G. C.; Yankner, B. A. *Nature* **1994**, *368*, 756.
(10) Zraika, S.; Hull, R. L.; Verchere, C. B.; Clark, A.; Potter, K. J.; Fraser, P. E.; Raleigh, D. P.; Kahn, S. E. *Diabetologia* **2010**, *53*, 1046.
(11) Gilead, S.; Gazit, E. *Exp. Diabetes Res.* **2008**, *2008*, 256954.
(12) Scrocchi, L. A.; Ha, K.; Chen, Y.; Wu, L.; Wang, F.; Fraser, P. E. *J. Struct. Biol.* **2003**, *141*, 218.
(13) Gazit, E. *Curr. Med. Chem.* **2002**, *9*, 1725.
(14) Nilsson, M. R.; Raleigh, D. P. *J. Mol. Biol.* **1999**, *294*, 1375.
(15) Ilitchev, A. I.; Giammona, M. J.; Do, T. D.; Wong, A. G.; Buratto, S. K.; Shea, J.-E.; Raleigh, D. P.; Bowers, M. T. *J. Am. Soc. Mass Spectrom.* **2016**, *27*, 1010.
(16) Kapurniotu, A.; Schmauder, A.; Tenidis, K. *J. Mol. Biol.* **2002**, *315*, 339.
(17) Tatarek-Nossol, M.; Yan, L. M.; Schmauder, A.; Tenidis, K.; Westermark, G.; Kapurniotu, A. *Chem. Biol.* **2005**, *12*, 797.
(18) Tenidis, K.; Waldner, M.; Bernhagen, J.; Fischle, W.; Bergmann, M.; Weber, M.; Merkle, M. L.; Voelter, W.; Brunner, H.; Kapurniotu, A. *J. Mol. Biol.* **2000**, *295*, 1055.
(19) Shim, S. H.; Gupta, R.; Ling, Y. L.; Strasfeld, D. B.; Raleigh, D. P.; Zanni, M. T. *Proc. Natl. Acad. Sci. U. S. A.* **2009**, *106*, 6614.
(20) Soriaga, A. B.; Sangwan, S.; Macdonald, R.; Sawaya, M. R.; Eisenberg, D. *J. Phys. Chem. B* **2016**, *120*, 5810.
(21) Deng, W.; Cao, A.; Lai, L. *Protein Sci.* **2008**, *17*, 1102.
(22) Azriel, R.; Gazit, E. *J. Biol. Chem.* **2001**, *276*, 34156.
(23) Cai, Z.; Li, J.; Yin, C.; Yang, Z.; Wu, J.; Zhou, R. *J. Phys. Chem. B* **2014**, *118*, 48.
(24) Melquiond, A.; Gelly, J.-C.; Mousseau, N.; Derreumaux, P. *J. Chem. Phys.* **2007**, *126*, 065101.
(25) Wu, C.; Lei, H.; Duan, Y. *Biophys. J.* **2005**, *88*, 2897.
(26) Wu, C.; Lei, H.; Duan, Y. *J. Am. Chem. Soc.* **2005**, *127*, 13530.
(27) Wu, C.; Lei, H.; Duan, Y. *Biophys. J.* **2004**, *87*, 3000.
(28) Zanuy, D.; Ma, B.; Nussinov, R. *Biophys. J.* **2003**, *84*, 1884.
(29) von Helden, G.; Hsu, M. T.; Gotts, N.; Bowers, M. T. *J. Phys. Chem.* **1993**, *97*, 8182.
(30) Dupuis, N. F.; Wu, C.; Shea, J.-E.; Bowers, M. T. *J. Am. Chem. Soc.* **2009**, *131*, 18283.
(31) Bernstein, S. L.; Dupuis, N. F.; Lazo, N. D.; Wyttenbach, T.; Condron, M. M.; Bitan, G.; Teplow, D. B.; Shea, J.-E.; Ruotolo, B. T.; Robinson, C. V.; Bowers, M. T. *Nat. Chem.* **2009**, *1*, 326.
(32) Cole, H. L.; Kalapothakis, J. M. D.; Bennett, G.; Barran, P. E.; MacPhee, C. E. *Angew. Chem., Int. Ed.* **2010**, *49*, 9448.
(33) Hoffmann, W.; von Helden, G.; Pagel, K. *Curr. Opin. Struct. Biol.* **2017**, *46*, 7.
(34) Baumketner, A.; Bernstein, S. L.; Wyttenbach, T.; Bitan, G.; Teplow, D. B.; Bowers, M. T.; Shea, J.-E. *Protein Sci.* **2006**, *15*, 420.
(35) Wyttenbach, T.; Grabenauer, M.; Thalassinos, K.; Scrivens, J. H.; Bowers, M. T. *J. Phys. Chem. B* **2010**, *114*, 437.
(36) Wyttenbach, T.; Bowers, M. T. *J. Phys. Chem. B* **2011**, *115*, 12266.
(37) Seo, J.; Hoffmann, W.; Warnke, S.; Bowers, M. T.; Pagel, K.; von Helden, G. *Angew. Chem., Int. Ed.* **2016**, *55*, 14173.
(38) Bleiholder, C.; Dupuis, N. F.; Wyttenbach, T.; Bowers, M. T. *Nat. Chem.* **2011**, *3*, 172.
(39) Economou, N. J.; Giammona, M. J.; Do, T. D.; Zheng, X.; Teplow, D. B.; Buratto, S. K.; Bowers, M. T. *J. Am. Chem. Soc.* **2016**, *138*, 1772.
(40) Warnke, S.; Seo, J.; Boschmans, J.; Sobott, F.; Scrivens, J. H.; Bleiholder, C.; Bowers, M. T.; Gewinner, S.; Schöllkopf, W.; Pagel, K.; von Helden, G. *J. Am. Chem. Soc.* **2015**, *137*, 4236.
(41) Barth, A. *Biochim. Biophys. Acta, Bioenerg.* **2007**, *1767*, 1073.
(42) Jackson, M.; Mantsch, H. H. *Crit. Rev. Biochem. Mol. Biol.* **1995**, *30*, 95.
(43) Seo, J.; Hoffmann, W.; Warnke, S.; Huang, X.; Gewinner, S.; Schöllkopf, W.; Bowers, M. T.; von Helden, G.; Pagel, K. *Nat. Chem.* **2017**, *9*, 39.
(44) Kayed, R.; Bernhagen, J.; Greenfield, N.; Sweimeh, K.; Brunner, H.; Voelter, W.; Kapurniotu, A. *J. Mol. Biol.* **1999**, *287*, 781.
(45) Wolfe, L. S.; Calabrese, M. F.; Nath, A.; Blaho, D. V.; Miranker, A. D.; Xiong, Y. *Proc. Natl. Acad. Sci. U. S. A.* **2010**, *107*, 16863.
(46) Warnke, S.; von Helden, G.; Pagel, K. *Proteomics* **2015**, *15*, 2804.
(47) Wang, L.; Ilitchev, A. I.; Giammona, M. J.; Li, F.; Buratto, S. K.; Bowers, M. T. *J. Phys. Chem. B* **2016**, *120*, 11905.
(48) Dupuis, N. F.; Wu, C.; Shea, J.-E.; Bowers, M. T. *J. Am. Chem. Soc.* **2011**, *133*, 7240.
(49) Lee, S. J. C.; Choi, T. S.; Lee, J. W.; Lee, H. J.; Mun, D.-G.; Akashi, S.; Lee, S.-W.; Lim, M. H.; Kim, H. I. *Chem. Sci.* **2016**, *7*, 5398.
(50) Young, L. M.; Cao, P.; Raleigh, D. P.; Ashcroft, A. E.; Radford, S. E. *J. Am. Chem. Soc.* **2014**, *136*, 660.
(51) Arrondo, J. L. R.; Goñi, F. M. *Prog. Biophys. Mol. Biol.* **1999**, *72*, 367.
(52) Bramanti, E.; Benedetti, E. *Biopolymers* **1996**, *38*, 639.
(53) Do, T. D.; LaPointe, N. E.; Nelson, R.; Krotee, P.; Hayden, E. Y.; Ulrich, B.; Quan, S.; Feinstein, S. C.; Teplow, D. B.; Eisenberg, D.; Shea, J.-E.; Bowers, M. T. *J. Am. Chem. Soc.* **2016**, *138*, 549.
(54) Bowers, M. T. *Int. J. Mass Spectrom.* **2014**, *370*, 75.
(55) Kemper, P. R.; Dupuis, N. F.; Bowers, M. T. *Int. J. Mass Spectrom.* **2009**, *287*, 46.

DOI: 10.1021/jacs.7b09510
J. Am. Chem. Soc. 2018, 140, 244−249